Simulation of groundwater drainage into a tunnel in fractured rock and numerical analysis of leakage remediation, Romeriksporten tunnel, Norway

N.-O. Kitterød · H. Colleuille · W.K. Wong
T.S. Pedersen

Abstract Standard geostatistical methods for simulation of heterogeneity were applied to the Romeriksporten tunnel in Norway, where water was leaking through high-permeable fracture zones into the tunnel while it was under construction, causing drainage problems on the surface. After the tunnel was completed, artificial infiltration of water into wells drilled from the tunnel was implemented to control the leakage. Synthetic heterogeneity was generated at a scale sufficiently small to simulate the effects of remedial actions that were proposed to control the leakage. The flow field depends on the variance of permeabilities and the covariance model used to generate the heterogeneity. Flow channeling is the most important flow mechanism if the variance of the permeability field is large compared to the expected value. This condition makes the tunnel leakage difficult to control. The main effects of permeability changes due to sealing injection are simulated by a simple perturbation of the log-normal probability density function of the permeability. If flow channeling is the major transport mechanism of water into the tunnel, implementation of artificial infiltration of water to control the leakage requires previous chemical-sealing injection to be successful.

Résumé Des méthodes géostatistiques standard ont été employées pour simuler l'hétérogénéité des zones de fractures à fortes perméabilitées dans lesquelles, au cours de la construction du tunnel ferroviaire de Romeriksporten (Norvège), l'eau s'est écoulée, causant des problèmes de drainage en surface. Quand les travaux ont été terminés, l'injection d'eau dans des puits forés à partir du tunnel a été réalisée pour contrôler ces infiltrations. Une hétérogénéité synthétique a été créée à une échelle suffisamment petite pour simuler les effets de l'injection d'eau. Le champ des écoulements dépend de la variance des perméabilités et de la covariance du modèle utilisé pour générer l'hétérogénéité. La chenalisation de l'écoulement est le mécanisme d'écoulement le plus important si la variance du champ de perméabilité est grande par rapport à la valeur moyenne. Cette condition fait que les infiltrations dans le tunnel sont difficiles à contrôler. L'étanchéification du tunnel par des produits chimiques est simulé par une simple perturbation de la fonction de densité de probabilité log-normale de la perméabilité. Si la chenalisation de l'écoulement est le principal mécanisme de transport d'eau entrant dans le tunnel, la création d'une injection artificielle de l'eau pour contrôler l'infiltration dans le tunnel impose, pour réussir, une imperméabilisation préalable par des produits chimiques.

Resumen Se han aplicado métodos estadísticos convencionales para la simulación de la heterogeneidad en el túnel de Roeriksporte (Noruega), donde la presencia de agua en zonas fracturadas de alta permeabilidad originó problemas de drenaje en superficie durante su construcción. Una vez finalizado el túnel, para controlar la infiltración se inyectó agua en los pozos situados en su interior. La generación del campo heterogéneo se realizó a una escala lo suficientemente pequeña que permitiera simular los efectos de las medidas de control propuestas. El campo de flujo depende de la varianza de las permeabilidades y del modelo de covarianza utilizado para generar la heterogeneidad. El flujo a través de canales es el mecanismo dominante si la varianza del campo de permeabilidad es grande en relación con el valor esperado. Este hecho condiciona que las filtraciones en el túnel sean difíciles de controlar. Los principales efectos de los cambios de permeabilidad originados por las inyecciones para el sellado del túnel se simularon mediante una simple perturbación de la función de densidad de probabilidad lognormal de la permeabilidad. Si el flujo a través de canales es el principal

Received: 12 April 1999 / Accepted: 22 May 2000
Published online: 23 September 2000

N.-O. Kitterød (✉) · W.K. Wong
University of Oslo, Department of Geophysics, P.O. Box 1022, Blindern, 0315 Oslo, Norway
E-mail: nilsotto@geofysikk.uio.no
Fax: +47-22-855269

H. Colleuille · T.S. Pedersen
Norwegian Water Resources and Energy Directorate, Hydrology Department, P.O. Box 5091, Majorstua, 0301 Oslo, Norway

 DOI 10.1007/s100400000089

mecanismo de la presencia de agua en el túnel, el control de las filtraciones mediante técnicas de inyección de agua en pozos de recarga requiere de la inyección previa de un producto químico para el sellado de las fisuras.

Key words fractured rocks · geostatistics · surface drainage · tunnel leakage · artificial infiltration

Introduction

The motivation for this study was a practical problem: water was leaking into a tunnel under construction, the Romeriksporten tunnel in Norway, causing technical, environmental, and economic problems. The east–west fracture zone creates hydraulic connections with the north–south fracture zones, which, when considered with the heterogeneity in the fracture zones, makes the leakage into the tunnel difficult to predict and to control. After tunnel construction was completed, damage due to groundwater drainage was documented (Gardermobanen 1998), and measures intended to control the leakage problem were suggested (Broch et al. 1997). The remediation method that was finally implemented is based on the so-called water-curtain principle (Kjørholt and Broch 1992; Broch and Kjørholt 1994), where water is injected through recharge wells drilled within the tunnel. This remediation technique was combined with previous injection of chemical sealing. To distinguish clearly between these two techniques, the term "injection" is reserved for chemical sealing and (artificial) "infiltration" for the water-curtain method.

Technical evaluation of leakage-remediation measures requires observations of small-scale heterogeneities. Unfortunately, such data are generally very expensive to acquire and were very sparse in this case. The purpose of this study was to generate a probable distribution of the permeabilities at a scale sufficiently small to be able to evaluate leakage remediation. To make the simulations as realistic as possible, surface observations were used to derive boundary conditions and average (large-scale) parameters for the small-scale flow simulation. The tunnel location and associated geology and fracture patterns are shown in Fig. 1.

Mathematical models describing flow in fractured rocks may be classified into three groups (National Research Council 1996): continuum models (Bear 1993); discrete-network models (Long and Billaux

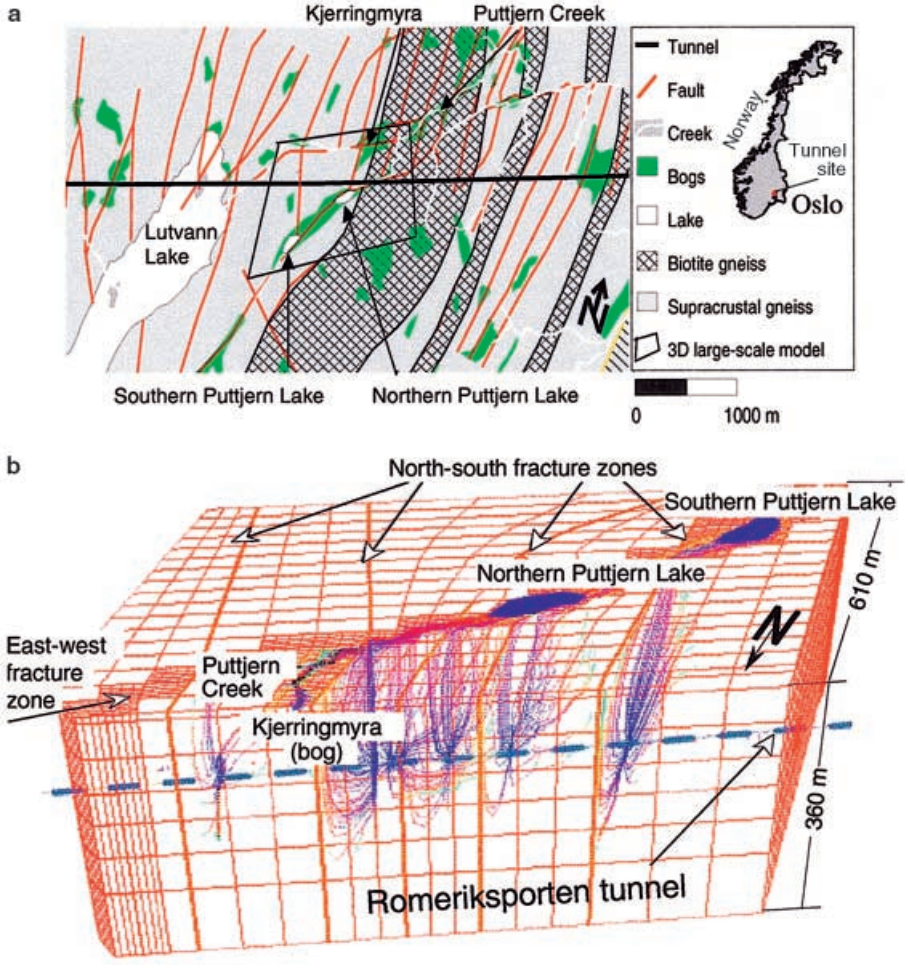

Fig. 1 Location of Romeriksporten tunnel, Norway. **a** Geological map of tunnel area, showing location of the 3D modeled area; **b** 3D flow field, indicating leakage from Northern and Southern Puttjern Lakes. *Streamlines* indicate transport time to tunnel: *blue* and *lilac* <10 d; *red* <40 d; *green* <90 d

 DOI 10.1007/s100400000089

1987; Clemo and Smith 1997); and hybrid models. In the hybrid models, the continuum approximation is usually based on discrete-network analysis. Independent of the flow model, different statistical models may be used to describe and simulate geometry of fractures and hydraulic properties. A family of widely used statistical models assumes fractal geometry (e.g., Mandelbrot 1971; Feder 1988; Odling 1997; Bour and Davy 1998), but other statistical models have also been developed and implemented for practical applications relevant in fractured rocks (Hjort and Omre 1993; Damsleth and Holden 1994). In particular, this study is inspired by Neretnieks' (1993) observations that led to the concept of flow channeling, or preferential flow in fractured rocks (Tsang and Neretnieks 1998). This paper focuses on the spatial variations of permeability in a fracture zone where leakage was monitored carefully. An assumption is that the permeability of a specified volume of the permeable fracture zone can be expressed as representative (average) numbers, and that these representative permeabilities can be modeled as continuous random functions. Furthermore, it is assumed that the permeability has a spatial correlation structure with finite variance, and the statistical character of the permeability field can be modeled as log-normal probability density functions (pdfs).

As indicated above, the simulation process consists of two parts, a regional (large-scale) flow modeling and a small-scale simulation of flow in individual fracture zones. The calibrated large-scale flow parameters reproduce the main hydrological observations for the field situation before the tunnel came into being and after the tunnel was constructed (Kitterød et al. 1998). The term "small-scale" in this paper denotes flow conditions in a permeable fracture zone spanning a few meters of the tunnel. The term "large-scale" refers to the area marked in Fig. 1b that corresponds to a rock volume of approximately 0.175 km^3 (770×630×360 m) and that includes five major fracture zones.

This paper summarizes the analysis of flow conditions in a single fracture zone. Different realizations of the permeability field are generated with high spatial resolution by using two different covariance functions. Afterward, water flow was simulated by using the boundary conditions based on the regional flow modeling. For each covariance model, four different variances were applied; thus no full Monte Carlo simulation was done in this project. The purpose is to show how flow channeling in a fracture zone depends both on the covariance model and on expectation and variance of a log-normal pdf. Given a covariance model, the magnitude of the variance is critical for technical remediation of the leakage into the tunnel.

Site Description

The method and simulation results presented in this paper are intended to be of general character, although to a large extent this is a site-specific study. For this reason a brief description of relevant geological and hydrological observations is given as an introduction.

Geological Setting

Romeriksporten tunnel (Fig. 1) is located close to the Oslo graben (Oftedahl 1981; Heimli 1994). The bedrock belongs to the southeastern Norwegian basement, generated during the Sweco-Norwegian orogenesis approximately 10^9 years ago (Graversen 1984). The fracture zones have two main directions, one north–south and the other more east–west. The most important fracture zones were probably generated during the Sweco-Norwegian orogenesis but have later been reactivated several times through the geological history, especially during the Permian tension at the time when the Oslo graben was generated. The latest event that is most important for the rock-mass permeability is the post-glacial isostatic rebound of the Scandinavian crust. In the model area, the present uplift rate is about 4 mm/year (Sørensen et al. 1997). A significant correlation between hard-rock permeability and magnitude of uplift is pointed out by Rohr-Torp (1994).

No detailed field mapping of the bedrock was performed prior to tunnel construction, but the most important fracture zones are easily seen on aerial photos and topographical maps. Logging of rock characteristics, including strike and dip of fracture zones and leakage from pre-drilling wells, was done as the tunnel construction progressed. In Kitterød et al. (1998), this information was used to generate a 3D gridnet where the fracture zones and faults were modeled as vertical 2D planes with 2-m thickness for the north–south fracture zones and 10-m thickness for the east–west fault zones (Fig. 1). The bedrock between the fracture zones is assumed to have low permeability. In this case, the average hydraulic conductivity of the bedrock was set equal to $K \approx 1 \times 10^{-9}$ m/s.

Hydrological Observations

No detailed analysis of the regional water balance was done prior to the tunnel construction, but observations initiated after construction are available in a publication by the Norwegian State Railways (1998). Estimates indicate a specific runoff in the area of about 1.3 mm/d (Norwegian Water Resources and Energy Directorate 1987). The local catchment area within the modeled domain (Fig. 1) is estimated to be 0.277 km^2, giving a recharge of 360 m^3/d.

Measurements of leakage in the most water-conductive sections of the tunnel indicate discharge of

 DOI 10.1007/s100400000089

more than 1000 m^3/d during extreme periods. This amount was reduced to about 240 m^3/d after injection of chemical sealing. These measurements were made in the section of the tunnel corresponding to the modeled area in Fig. 1, which includes about 700 m of the tunnel.

Measurements of hydraulic head indicate the geological heterogeneity of the area. In some positions the measured drawdown in wells was 40–50 m, whereas in other observation wells located equally close to the tunnel no significant drawdown was recorded. A qualitative tracer test was also performed (Pedersen 1997). Tracers were applied in shallow injection wells located in Northern Puttjern Lake, where a major fracture zone intersects the lake and the tunnel. The breakthrough was observed after less than 5 h, with maximum concentration occurring after 25 h. The vertical travel distance is about 200 m, which indicates a significant hydraulic communication between the surface and the tunnel. Results of this tracer test are used later in this paper as an argument for applying a spatial correlation length of the permeabilities in the fracture zone with the same order of magnitude as the vertical distance between the surface and the tunnel. Northern Puttjern Lake was nearly drained during the tunnel construction, and significant drainage was also observed in the boggy area called Kjerringmyra (Fig. 1b).

Leakage Remediation

Injection of chemical sealing was the main measure that was taken to prevent leakage. This injection was done during the construction and after the tunnel was completed. However, the leakage was still above the acceptable level. To prevent permanent drainage of surface water, water-infiltration equipment was installed in the tunnel. Eighteen injection wells, each with a diameter of 100 mm, were drilled in the areas with most fractures. The penetration length of these wells ranged from 12–70 m. The wells were arranged in a fan-shape to provide a maximum coverage of the adjacent fractured rock. The orientation of the wells differs, ranging from almost parallel to the axis of the tunnel to an angle at 45°. When the infiltration system is in operation, 400 l/s of water are pumped into the fractures at a pressure of approximately 18 bars. The system is designed to be used only when the groundwater level declines to a predefined critical level.

Method of Analysis

The analysis of fluid flow around and into a tunnel constructed in fractured rocks is extremely complex and involves several fluid phases. In addition, fractured rock is usually very heterogeneous; thus for realistic computations of flow it is necessary to construct a 3D network. This requirement puts severe demands on the flow computations with respect to numerical capacity. A method called front tracking (Bratvedt et al. 1992, 1994) is numerically efficient and can handle complex geometries. The method is implemented in FRONTSIM (GeoQuest 1998), which was used in this project to solve the 3D regional flow (Kitterød et al. 1998) and the local 2D flow for individual fracture zones. Multiphase flow was not considered in this study, and thus only the equations describing single-phase water flow governed by Darcy's law are discussed. Subsequently, the application of stochastic simulation is presented and how such methods may be used to include effects of heterogeneous permeability is discussed.

Flow Computations

Both the fluid and the fractured rock are considered to be incompressible, i.e., porosity n and density of the water ρ are constant in time t. The governing flow equation can then be written:

$$n\rho\frac{\partial}{\partial t}(S) - \rho\nabla\cdot\left[\frac{k\rho g}{\mu}\nabla\left\{\frac{P}{\rho g} - z\right\}\right] = -\Gamma \qquad (1)$$

where S is saturation, k is permeability, g is acceleration of gravity, P is pressure, z is depth below surface, Γ is source-sink term, and

$$\nabla = \left(\frac{\partial}{\partial x}, \frac{\partial}{\partial y}, \frac{\partial}{\partial z}\right).$$

The next simplification is to let $\partial S/\partial t=0$, i.e., saturation does not change with time. Then Eq. (1) may be written:

$$\nabla\cdot[K\nabla\varphi] = \frac{\Gamma}{\rho} \qquad (2)$$

where $K=k\rho g/\mu$ and is called hydraulic conductivity [L/T], and $\varphi=P/\rho g-z$ is hydraulic head [L]. Γ describes precipitation and evaporation processes, which usually vary with time; hence, $\Gamma=\Gamma(t)$. However, in this case Γ=constant, and because the effect of compressibility is ignored and only saturated flow is considered, Eq. (2) describes stationary flow. The inverse problem is to estimate K by finding solutions of Eqs. (1) or (2) that are consistent with observations of Γ and φ. In Kitterød et al. (1998), this estimate was made by manual calibration of homogeneous permeability of the fracture zones. In the present study, K is treated as a stochastic function, and Eq. (2) is used to find the flux response with different realizations of K as input.

Stochastic Simulation of Heterogeneity

Though Eq. (2) is simple to solve from a numerical point of view, it is a challenge to describe the spatial variation of K that represents the hydraulic conductivity for a given element volume V. In this case study,

 DOI 10.1007/s100400000089

the flow domain is discretized to a regular grid: $V=(\Delta x\times\Delta y\times\Delta z)$. In the general case, K is a 3×3 tensor, but in this case no observations indicate anisotropy; hence, isotropic K is assumed. The size of V determines the total variance of K and thereby also what statistical models are the most suitable. If V increases, the variance of K decreases, but at the same time the spatial correlation length R increases. This phenomenon is called regularization and is treated by Dagan (1989), Journel and Huijbregts (1989), and others. The hydraulic conductivity K is modeled as a continuous stochastic function with multivariate log-normal pdf, i.e., $X=\ln K$, where X is distributed as $N[\mu_X,Cov_X]$, where $E[X(\mathbf{u})]=\mu_X$, $Cov_X(\mathbf{u},\mathbf{u}')=Cov_X$, and $\mathbf{u}$ and $\mathbf{u}'$ denote positions in space. The assumption of multivariate log-normal K is crucial in this study, and there is an ongoing discussion on which statistical model is most suitable for fractured rocks (e.g., Bear et al. 1993; National Research Council 1996).

In this study, unconditional realizations of $X(\xi,\mathbf{u})=\sigma_X Z(\xi,\mathbf{u})+\mu_X$ are simulated, where $Z(\xi,\mathbf{u})$ is generated by expanding a predefined covariance function $Cov[Z(\xi,\mathbf{u}), Z(\xi,\mathbf{u}')]$ into a series of eigenvalues λ and eigenfunctions $\beta(\mathbf{u})$:

$$\int_V Cov[Z(\xi,\mathbf{u}),Z(\xi,\mathbf{u}')]\beta_i(\mathbf{u}')d\mathbf{u}'=\lambda_i\beta_i(\mathbf{u})i=1,...,\infty \quad (3)$$

where ξ indicates the realization. The eigenfunctions and eigenvalues are conditioned so that:

$$\int_V \beta_i(\mathbf{u})\beta_j(\mathbf{u})d\mathbf{u}=\delta_{ij} \quad (4)$$

and

$$E\left[\Phi_i(\xi)\Phi_j(\xi)\right]=\delta_{ij}\lambda_i \quad (5)$$

where δ_{ij} is the Kronecker delta ($\delta_{ij}=1$ if i=j; otherwise, $\delta_{ij}=0$), and Φ are stochastic coefficients.

$Z(\xi,\mathbf{u})$ was then computed in terms of eigenfunctions and stochastic coefficients according to the Karhunen-Loève theorem (e.g., Davenport and Root 1958; Christakos 1992). If the expansion is truncated at m number of eigenfunctions, the simulation algorithm is written:

$$Z(\xi,\mathbf{u})=\sum_{i=1}^{m}\beta_i(\mathbf{u})\Phi_i(\xi)+\varepsilon(\xi) \quad (6)$$

where the white noise term $\varepsilon(\xi)$ is the residual variance corresponding to the nugget effect where the spatial covariance is ignored. In this case, the expansion of eigenfunctions is truncated at 99.5% of $Var[Z(\xi,\mathbf{u})]$; for more details see Kitterød and Gottschalk (1997).

The simulation algorithm in Eq. (6) can be used to simulate a non-stationary stochastic process (Braud and Obled 1991). In this case, no information was available to indicate spatial changes in the statistical moments. Thus, $Z(\xi,\mathbf{u})$ was simplified to a second-order stationary process, i.e., $E[Z(\xi,\mathbf{u})]=E[Z]$ and $Cov[Z(\xi,\mathbf{u}), Z(\xi,\mathbf{u}')]=Cov_Z(h)$, where $h=|\mathbf{u}-\mathbf{u}'|$. No direct observations were available to support the choice of covariance model. Thus a simple exponential model $Cov_Z(h)=\exp[-\alpha h^n]$ was applied. The value of n determines the spatial smoothness of $Z(\xi,\mathbf{u})$. The first-order exponential model (n=1) results in rough fields, whereas the second-order exponential model (n=2) gives smooth fields. In the following, the 'first-order exponential' model is called 'exponential' and the 'second-order exponential' model is called 'Gaussian'. To obtain the same practical range R for the two models, let $Cov_Z(R)=0.05$, giving $\alpha=\ln(20)/R^n$. Expanding the covariance functions in terms of eigenfunctions and eigenvalues, the two models (n=1 and n=2) represent extremes with respect to convergence of variance (Kitterød and Gottschalk 1997). Realizations of $Z(\xi,\mathbf{u})$ were generated in a regular 2D gridnet with spatial resolution $\Delta\mathbf{u}=(\Delta x,\Delta z)$; in the case study, $\Delta x=\Delta z=5$ m.

Numerical flow experiments were performed on six different realizations, three based on the exponential model and three on the Gaussian model. The experimental semivariograms ${}^*\gamma_Z(h)=1-{}^*Cov_Z(h)$ for the two models are shown in Fig. 2. The relation between the statistical moments for K and X is (e.g., Christakos 1992; Gottschalk 1995):

$$E[K(\xi,\mathbf{u})]=\mu_K=\exp\left(\mu_X+\frac{\sigma_X^2}{2}\right) \quad (7)$$

and

$$Cov_K(h)=\mu_K^2[\exp\{Cov_X(h)\}-1] \quad (8)$$

As soon as the values of σ_K and μ_K are available, σ_X and μ_X can be obtained from Eqs. (7) and (8), because $\mathrm{Cov}(0)=\sigma^2$. Unconditional realizations of hydraulic conductivity $K(\xi,\mathbf{u})$ are finally produced by:

$$K(\xi,\mathbf{u})=\exp\{\sigma_X Z(\xi,\mathbf{u})+\mu_X\}. \quad (9)$$

In this study, μ_K is equal to the calibrated average hydraulic conductivity, K_o, from the regional flow simulation (Kitterød et al. 1998), and four different values of σ_K are applied for each covariance model: $\sigma_K=0.5$, 1, 2, or $4\,\mu_K$. The probability density functions are shown in Fig. 3. According to the ergodic hypothesis, inference on all statistical moments can be made based on information from one single realization. Spatial averages for each realization demonstrate that the synthetic hydraulic conductivity generated for this case study behaves according to the ergodic hypothesis, as shown in Fig. 4. Because each field is made of a regular grid, the spatial average M_p for realization ξ is:

$$M_p(\xi)=\left(\frac{K^p(\xi,\mathbf{u}_1)+\cdots+K^p(\xi,\mathbf{u}_n)}{n}\right)^p \quad (10)$$

 DOI 10.1007/s100400000089

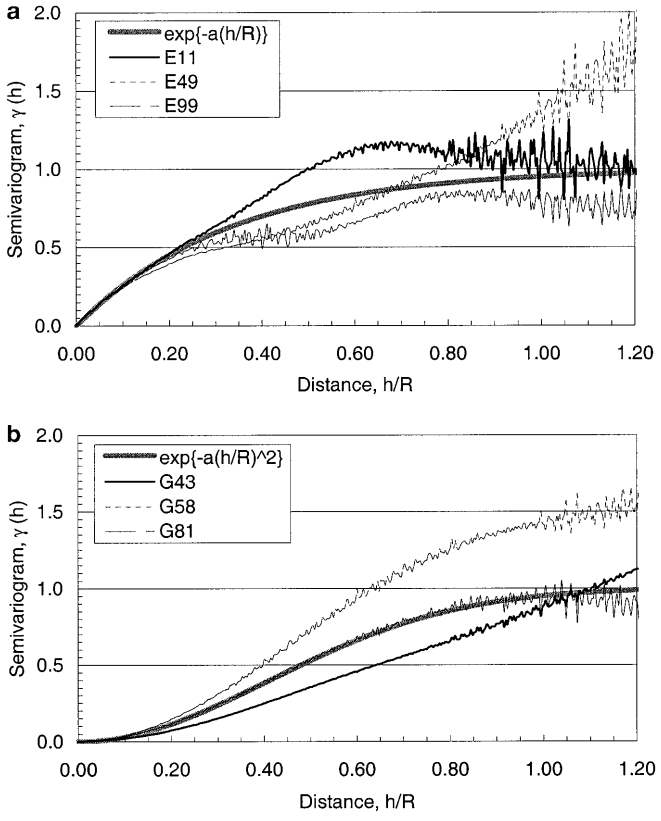

Fig. 2 Semivariograms γ(h) for six realizations plotted as a function of distance h=|**u**-**u**′|, where **u** and **u**′ indicate positions in space. *X-axis* is standardized with respect to practical range R. Realizations are generated with **a** exponential semivariogram models and **b** Gaussian semivariogram models. Analytical models are indicated in *bold gray lines*

where $\mathbf{u}_1,...,\mathbf{u}_n$ denotes all positions in the lattice, p=1 is the arithmetic mean, p=2 is the root mean square, and p=–1 is the harmonic mean. The geometric mean is:

$$M_g(\xi) = \{K(\xi,\mathbf{u}_1)K(\xi,\mathbf{u}_2)\cdots K(\xi,\mathbf{u}_n)\}^{1/n} \qquad (11)$$

For a normal pdf with $Cov_X(h)$=exp[-α h^n], the practical range R, defined as $Cov_X(R)$=0.05, is independent of the variance if α=ln(20)/R^n. By keeping α constant, an equivalent definition of $Cov_K(R')$=0.05, where K belongs to a log-normal pdf, results in a practical range R' that depends on both the covariance model and the variance. In this case, let σ_K={0.5, 1, 2, 3, 4 μ_K}, which gives corresponding relative ranges R'/R={0.97, 0.89, 073, 0.53} for the exponential covariance model, and R'/R={0.99, 0.95, 086, 0.73} for the Gaussian covariance model; relationships are shown in Fig. 5.

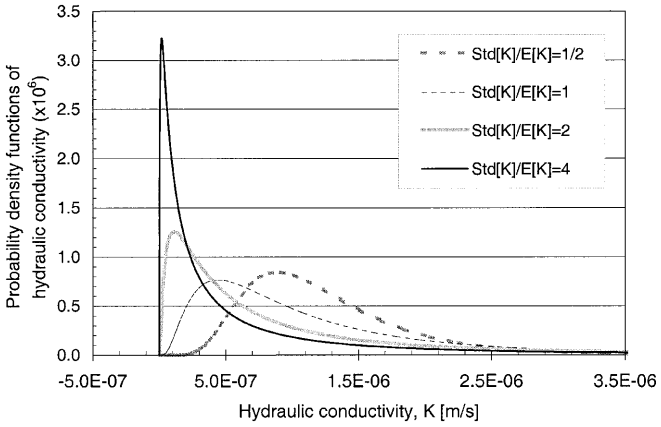

Fig. 3 Four log-normal probability density functions with constant expectation of hydraulic conductivity K, $E[K]$=μ_K=1.25×10^{-6} m/s, but with increasing standard deviation $std[K]$=σ_K=0.5, 1, 2, and 4 times $E[K]$

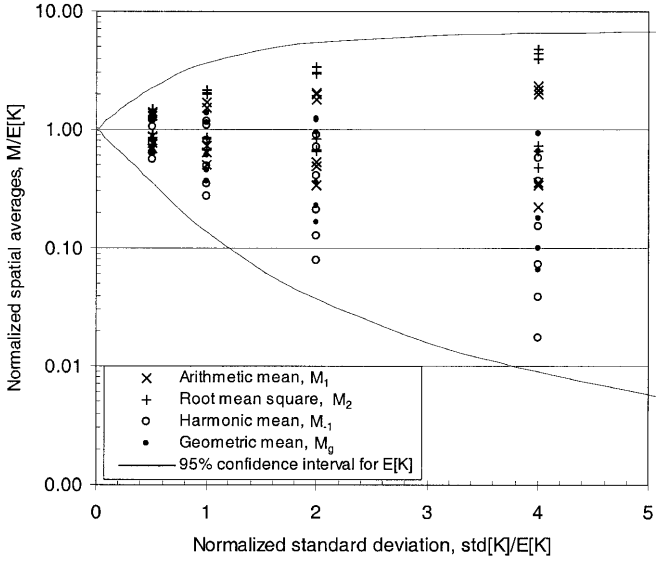

Fig. 4 Spatial averages of hydraulic conductivity M over model domain plotted as a function of increasing standard deviation standardized with respect to expected value of hydraulic conductivity

Simulation Setup

As mentioned above, the starting point for the 2D simulation is a regional 3D flow model (Fig. 1). In the 3D modeling, each fracture zone is regarded as homogeneous. The main features of the observed flow conditions (water balance, regional groundwater pressure) were reproduced by the same set of hydraulic parameters for the situation before and after tunnel construction, including the tracer test. These results were achieved by an average porosity of 1% and hydraulic conductivities of 2.5×10^{-7} to 1.3×10^{-6} m/s in the fracture zones. The transmissivity of the fracture zones is typically 2.5×10^{-6} m^2/s, where the width W is

 DOI 10.1007/s100400000089

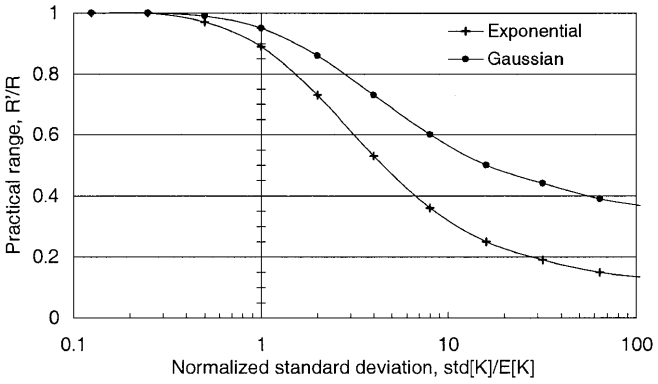

Fig. 5 Practical range R' for a hydraulic conductivity K, plotted as a function of increasing standard deviation $std[K]=\sigma_K$ for an exponential and a Gaussian semivariogram model. R' is standardized with respect to practical range R for $X=\ln K$, and $std[K]$ is standardized with respect to expected value of K, which is kept constant, $E[K]=\mu_K=1.25\times10^{-6}$ m/s. The stochastic function K has a log-normal probability density distribution

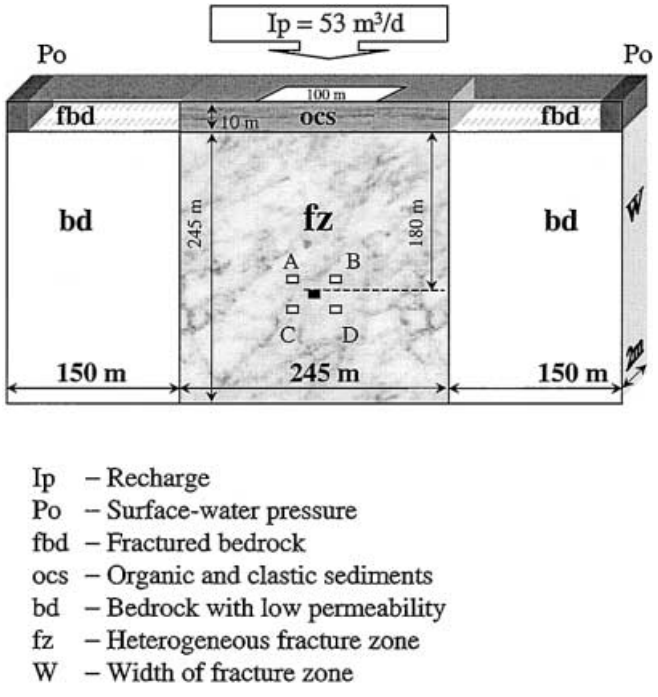

Fig. 6 Setup for simulation of groundwater flow: boundary condition with recharge $I_p=53\,m^3/d$, and $P_0=1$ bar representing surface-water pressure. Except for the infiltration area, all external boundaries are impervious. Tunnel cross section is indicated as a *black square* (5×5 m) with infiltration wells A, B, C, and D placed symmetrically around it

2–10 m (Kitterød et al. 1998). The 2D simulations were performed on an idealized cross section perpendicular to the tunnel, shown in Fig. 6, where the homogeneous fracture in the 3D model is substituted by heterogeneous permeability fields fz, generated according to Eq. (9). Let W=2 m; thus Eq. (7) is $E[K(\xi,\mathbf{u})]=K_0=1.25\times10^{-6}$ m/s for all realizations.

Boundary conditions and geological elements are illustrated in Fig. 6. The most reliable observation in this case study is measurements of leakage discharge. However, it is impossible to deduce average water flux through one single fracture zone directly from the available measurements. Average flow was taken from the 3D simulations in Kitterød et al. (1998), which gave a steady-state discharge of 120 m^3/d through the two most conductive fracture zones, where approximately 40 m^3/d was coming from the boggy land Kjerringmyra (Fig. 1b). In the 2D analysis, the main focus is heterogeneity. Consequently, the 3D geometry was simplified to a symmetrical problem, which implies that the Kjerringmyra source is modeled as two parallel constant heads in 2D. At the same time, it was important to maintain the ratio of (1) water coming from Kjerringmyra to (2) the total leakage into the tunnel, i.e., 40/120=1/3. This is achieved by a discharge of 80 m^3/d through one single fracture zone and with a recharge I_p from net infiltration equal to 53 m^3/d. A leakage of 80 m^3/d through one fracture zone corresponds approximately to 400 m^3/d in the 3D modeled area (Fig. 1a), which agrees well with measurements representing the same section of the tunnel. Thus I_p is set deterministically to 53 m^3/d and is applied in the central part of the model corresponding to the Northern Puttjern Lake (Fig. 1). The boggy land is represented by a reference pressure $P_0=1$ bar at the two corner nodes in the upper part of the model. All other boundaries are no-flow. The tunnel is also specified as a pressure condition $P_0=1$ bar corresponding to atmospheric pressure. The same is true for the infiltration points A, B, C, and D, where the intended injection pressure is specified to 2 bars above hydrostatic pressure. The model consists of three geological elements in addition to the heterogeneous fracture zone fz (Fig. 6): (1) two relatively impervious bedrock units (bd) with hydraulic conductivity set equal to 1×10^{-9} m/s; (2) a top unit of organic and clastic sediments (ocs); and (3) two permeable fractured-bedrock units (fbd) with extensive horizontal fractures. The permeabilities in fbd and ocs were calibrated to obtain pressure conditions corresponding as closely as possible to observations and at the same time having an average tunnel leakage equal to $Q_0=80\,m^3$/d. For homogeneous fz, the hydraulic conductivity of fbd is calibrated to 2.4×10^{-4} m/s and ocs to 8.5×10^{-4} m/s.

Results of Computations

Three situations are simulated for each realization of fz: (1) natural flow prior to tunnel construction; (2) flow after tunnel construction; and (3) conditions after implementation of artificial infiltration in A, B, C, and D (Fig. 6). Realizations based on exponential covariance model are named E11, E49, and E99, and Gaussian realizations are named G43, G58, and G81. The differences between the two models are shown in

 DOI 10.1007/s100400000089

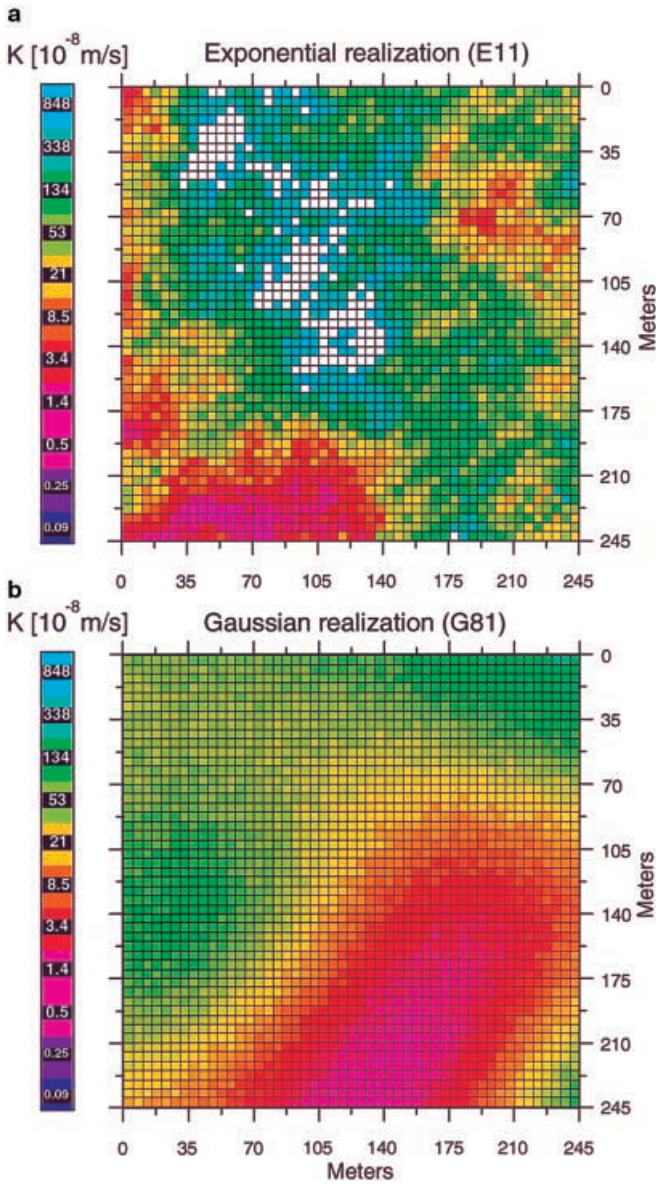

Fig. 7 Realizations of heterogeneous fracture zone generated with **a** exponential model (E11) and **b** Gaussian semivariogram model (G81), both with standard deviation *std*[*K*] equal to 4 times *E*[*K*]. *White areas* in exponential realization indicate hydraulic conductivities exceeding 8.48×10^{-6} m/s

Fig. 7. Intuitively, the realizations based on the exponential model may seem to be more realistic for permeabilities of a fracture zone because of roughness, but in principle the visual appearance of effective permeabilities representing rock volumes of 5×2×5 m is unknown. Therefore realizations based on both models were included in the simulations.

Simulation of leakage into the tunnel without any artificial infiltration and without any calibration of permeabilities in fbd (Fig. 6) shows that discharge generally decreases as a function of increasing variance; results are shown in Table 1. This is true for all realizations except for E11, indicating the importance of tunnel position relative to the highly conductive flow paths. Plotting discharge of leakage water as a function of spatial averages, as shown in Fig. 8, demonstrates that a leakage reduction coincides with the geometric or harmonic mean, whereas an increase is better indicated by the arithmetic mean. The reason is probably that the harmonic and geometric means put more weight to low values than do the arithmetic mean and root mean square.

Four locations of artificial infiltration of water were simulated, each with a pressure P_c=2 bars above hydrostatic pressure. The water-infiltration points are located symmetrically above and below the tunnel at a distance of 14 m from the tunnel (Fig. 6). The results given in Tables 1 and 2 show that the effect of water-infiltration depends on the location of the infiltration points, the variance of the hydraulic conductivity, and the spatial distribution of the highly conductive flow paths. In Table 1, leakage reduction is given as a relative number Q/Q_0, where Q_0 is simulated tunnel leakage with homogeneous hydraulic conductivity in the fracture zone (Q_0=80 m^3/d). For each case, the water consumption giving a leakage reduction of 100 m^3/d is computed as well as changes in hydraulic head at the surface. In Table 2, effective leakage reduction (x) is computed by taking the difference between the flux into the tunnel Q_t and the water consumption for each case Q_i and relating the difference to tunnel leakage before artificial infiltration of water Q_p was implemented, i.e., $x=1-(Q_t-Q_i)/Qp$. The efficiency of water-infiltration for each realization is quite similar for the homogeneous field and for fields with low standard deviation (σ_K=0.5 μ_K); for these fields, the results are independent of the location of the infiltration wells (Table 2). In contrast, for realizations with high standard deviation (σ_K=4 μ_K), the positions of infiltration wells are very important, as shown for wells A and B, which are positioned differently with respect to the tunnel, as illustrated in Fig. 9.

The probability of short-circuiting water from the infiltration wells to the surface increases with increasing standard deviation if infiltration points are connected to highly conductive channels, which in turn implies that water is simply pumped from the tunnel to the surface. These conditions are illustrated in Fig. 10.

As shown in Table 1, the main result of the simulations is that groundwater pressure may be maintained and surface drainage prevented, but the water consumption may be substantial.

Discussion of Results

Two main approaches are commonly used to simulate geometry and hydraulic properties in fractured rocks: (1) discrete-network models, and (2) models based on representative average numbers. The latter rely on the

 DOI 10.1007/s100400000089

Table 1 Results of numerical simulations

Realization[a]	δ_K/μ_K[b]	Ratio of simulated tunnel leakage to leakage for homogeneous case[c] (Q/Q_0)	Relative water consumption[d] (m^3/d)	Relative head after tunnel construction (m)	Relative head after infiltration in four wells (m)
Homogeneous field	0	1.00	309	–5.6	5.6
E11	0.5	1.55	349	–8.8	8.7
	1	1.92	371	–11.0	10.7
	2	2.18	387	–12.4	12.1
	4	2.12	390	–12.1	11.7
E49	0.5	0.58	256	–3.3	3.4
	1	0.33	221	–1.8	1.9
	2	0.14	188	–0.7	0.8
	4	0.05	165	–0.2	0.3
E99	0.5	1.11	246	–6.2	6.4
	1	1.00	212	–5.7	5.6
	2	0.73	182	–4.1	4.5
	4	0.44	161	–2.5	2.9
G43	0.5	1.17	315	–6.3	6.3
	1	1.15	315	–6.4	6.3
	2	0.96	311	–5.3	5.3
	4	0.68	304	–3.7	3.7
G58	0.5	0.75	491	–4.2	4.2
	1	0.46	790	–2.5	2.5
	2	0.19	1598	–1.0	1.0
	4	0.06	3734	–0.3	0.3
G81	0.5	0.73	243	–4.1	4.1
	1	0.48	209	–2.7	2.7
	2	0.23	181	–1.3	1.3
	4	0.10	162	–0.5	0.5

[a] E, exponential semivariogram model; G, Gaussian semivariogram model
[b] standard deviation divided by expectation
[c] Q_0 (leakage for the homogeneous case)=80 m^3/d
[d] Water consumption related to a leakage reduction of 100 m^3/d

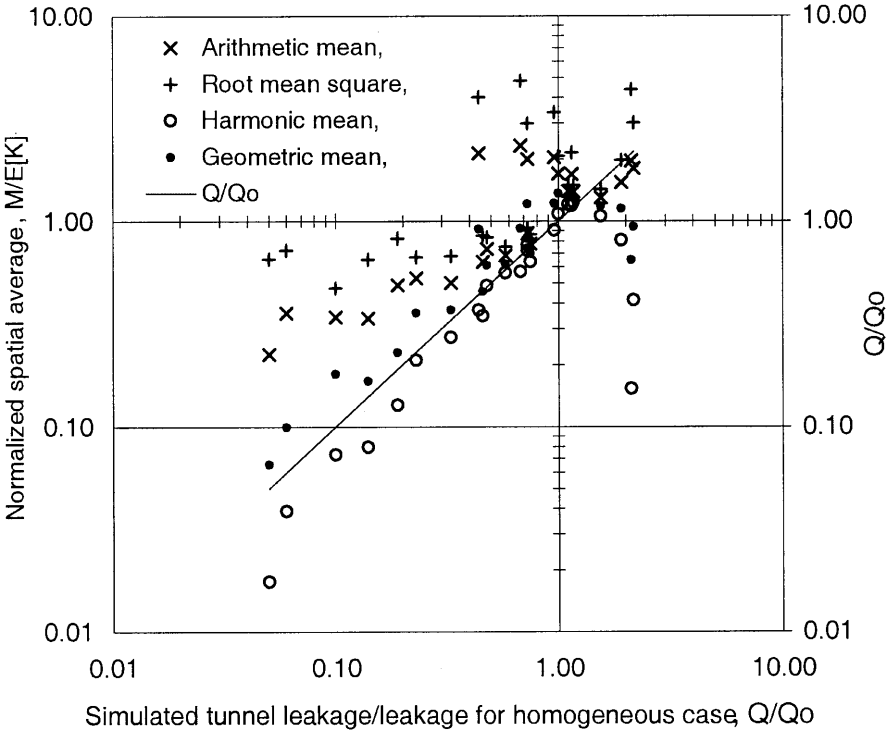

Fig. 8 Spatial averages of hydraulic conductivity M plotted as a function of simulated specific leakage Q. M is normalized with respect to expected value of hydraulic conductivity $E[K]=1.25\times10^{-6}$ m/s, and Q is normalized with respect to simulated leakage from a homogeneous fracture zone $Q_0=80\ m^3/d$

 DOI 10.1007/s100400000089

Table 2 Simulated amount of effective reduction of leakage into tunnel due to artificial infiltration of water in boreholes. Most successful (highest %) and least successful (lowest %) cases for each realization are indicated by bold values

Realization	δ_K/μ_K[a]	Effective reduction in leakage due to infiltration into borehole (%)				
		A	B	C	D	All four boreholes
Homogeneous field	0	49	49	45	45	99
E11	0.5	55	51	38	41	98
	1	59	51	34	37	98
	2	63	52	29	34	97
	4	**67**	52	**25**	31	97
E49	0.5	59	44	55	49	103
	1	66	40	61	52	106
	2	73	34	69	56	111
	4	**81**	**28**	78	60	117
E99	0.5	55	49	53	41	102
	1	59	48	59	37	105
	2	65	46	67	32	109
	4	**71**	44	74	**28**	114
G43	0.5	45	51	45	50	99
	1	42	52	44	54	99
	2	39	53	44	58	100
	4	**35**	53	43	**62**	100
G58	0.5	55	50	50	44	99
	1	59	50	54	43	99
	2	**62**	50	57	40	99
	4	60	43	55	**32**	98
G81	0.5	52	45	44	37	99
	1	55	42	43	31	99
	2	57	38	41	26	100
	4	**59**	34	40	**21**	101

[a] Standard deviation divided by expectation

continuum approach, which assumes that a representative elementary volume can be defined either in a literal sense (Bear 1993) or indirectly by convolution integrals (Baveye and Sposito 1984). In this paper, the focus is on flow in limited zones where tectonic activity has caused extremely high spatial frequency of interconnected fractures in all directions. In these zones, a discrete-network simulation is not adequate. Hence, the only feasible way to quantify hydraulic properties is by representative average numbers. In this case study, the length scale $\Delta\omega$ of the elementary volume is set equal to 5 m, which implies that the integral scale $I_h << \Delta\omega$. Gelhar (1987) reports 0.2 m$<I_h<$1 m derived from tracer studies in the Fennoscandian shield. The travel distance was approximately 10 m, but the tracer tests were performed in low-permeable rocks and the results cannot be transferred to high-permeable fracture zones without precautions. In the case study, the assumption is made that a calibrated hydraulic conductivity K_o that represents the modeled fracture zone with a length scale D=245 m can be considered as the expected value, i.e., $E[K(\xi,\mathbf{u})]=K_o$. This assumption is valid if hydraulic conductivity can be modeled as an ergodic and stationary stochastic function. The critical parameter at this scale (D=245 m) is the regularized integral scale I_X. Regularization implies a reduction of variance and an increase of correlation length, as given by the relation (Dagan 1989):

$$\frac{I_X}{I_h} = \left\{\frac{\sigma_h^2}{\sigma_X^2}\right\}^{1/m} \tag{12}$$

where m indicates space dimension, and σ_h and σ_X are standard deviation of $X=\ln K$ at length scale $\Delta\omega$ and D, respectively. A further assumption is that the spatial correlation structure of the regularized stochastic function X can be expressed as an exponential covariance function: $Cov_X(h)=\exp[-\alpha\ h^n]$. Applying Dagan's (1989) definitions of exponential and Gaussian covariance functions gives $I_X=1/\alpha$ for the exponential model (n=1) and $I_X=1/2(\pi/\alpha)^{1/2}$ for the Gaussian model (n=2). Defining the practical range R as $Cov_X(R)=0.05$ gives $\alpha=\ln(20)/R^n$. The critical question, still a subject of debate, is the size of R. The only observation available is the qualitative tracer test with a travel path from the Northern Puttjern Lake to the tunnel (Fig. 1) with a breakthrough time of less than 5 h. This result is the basis for applying a practical range with the same order of magnitude as the vertical travel distance, i.e., R=200 m. This value gives $I_X \approx 67$ m for the exponential model and $I_X \approx 102$ m for the Gaussian model. To invoke ergodicity and stationarity arguments, the condition D$>>I_X$ has to be met (Dagan 1989). Even though the choice of parameter values may be considered at the outer limit for the real fracture zone, Fig. 4 justifies that ergodicity and stationarity are valid assumptions for the synthetic fields generated for this case study.

 DOI 10.1007/s100400000089

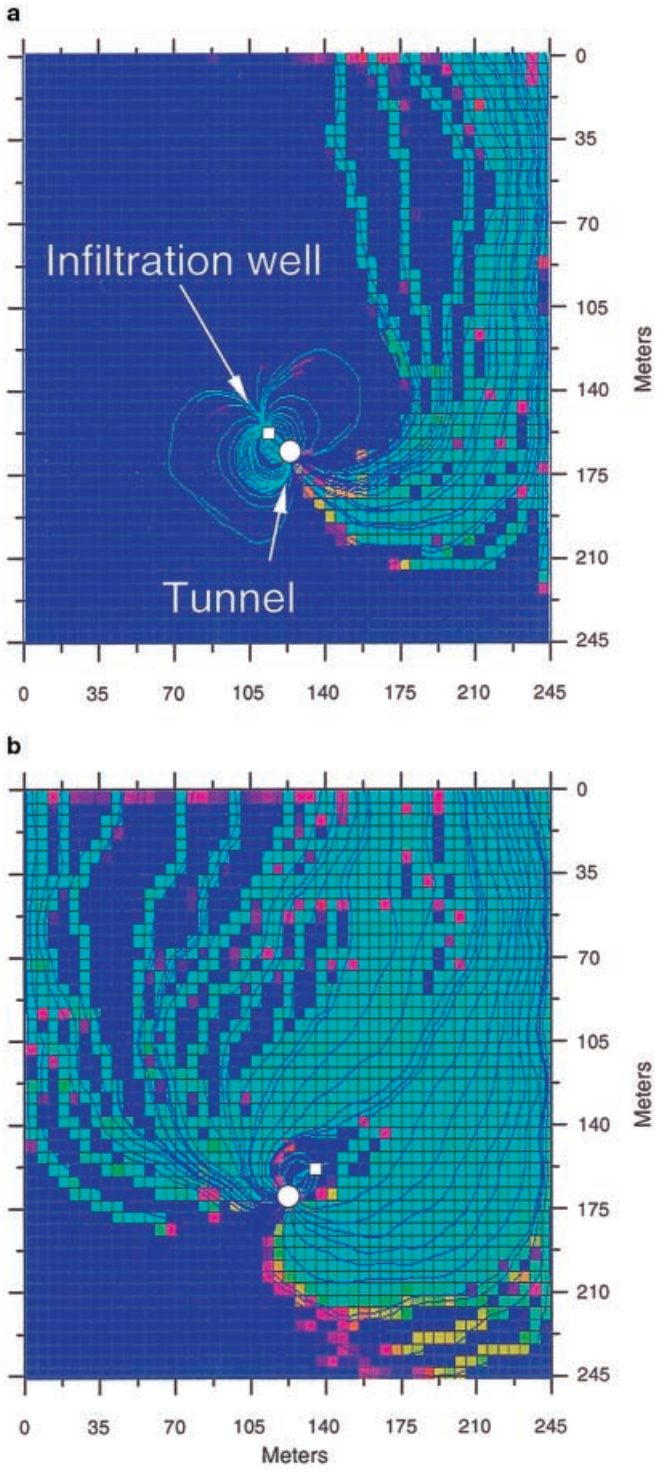

Fig. 9 Two locations of artificial infiltration of water for realization E49 with standard deviation *std*[*K*] equal to 4 times *E*[*K*]. *Dark blue streamlines on light blue pixels* indicate surface water leaking into tunnel; *light blue streamlines on dark blue pixels* indicate flow from artificial infiltration. **a** Water infiltrated in borehole location A (Fig. 6), which gives an effective leakage reduction of 81%; **b** Water infiltrated in borehole location B (Fig. 6), which gives an effective leakage reduction of 28%

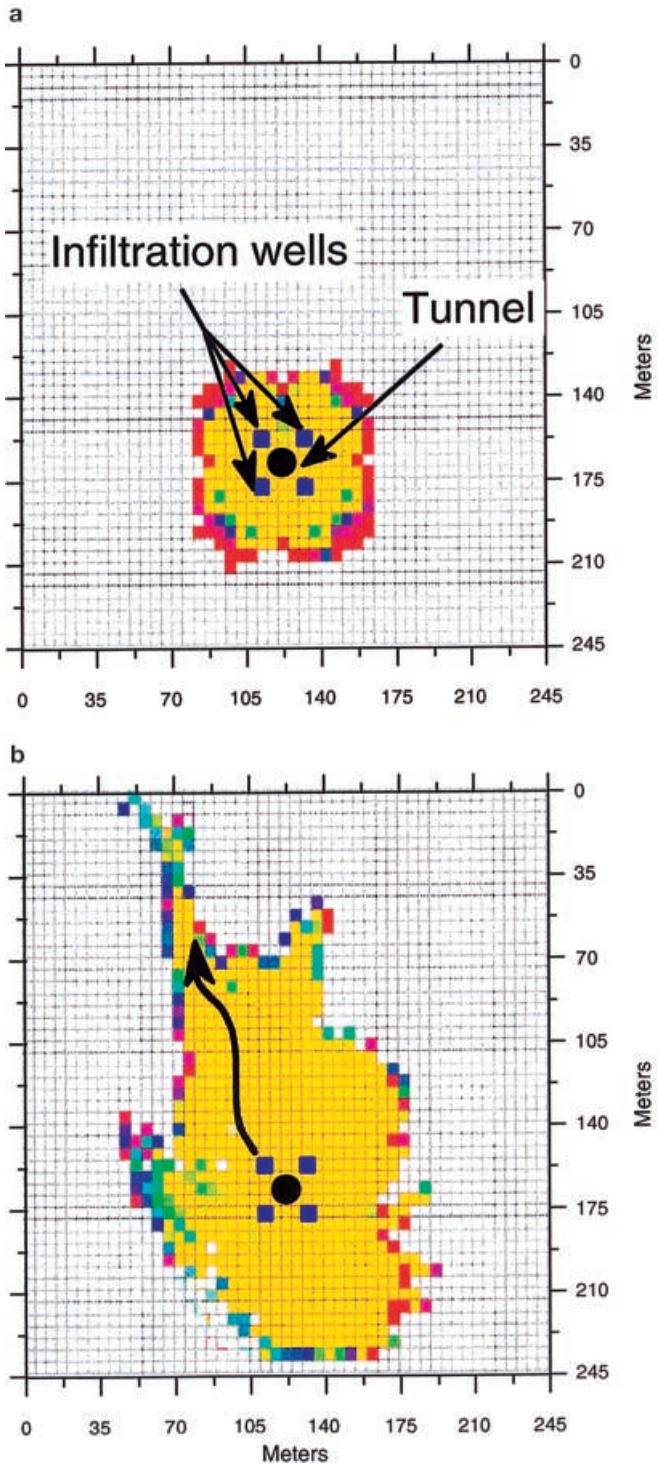

Fig. 10 Water infiltration from four bore holes in **a** homogeneous fracture zone and **b** heterogeneous fracture zone (E99, *std*[*K*]=4*E*[*K*]). *Yellow pixels* indicate region where all the water is coming from infiltration wells. *Other colors* indicate mixing of water from surface and infiltration wells

 DOI 10.1007/s100400000089

In this study, the correlation length R of the normal variable X was kept constant, which implies that the correlation length R' of the hydraulic conductivity $K=\exp(X)$ decreased as a function of increasing variance, as shown in Fig. 5. A subject for further study would be to keep R' constant by adjusting R. Another appropriate topic for further studies would be to assess the impact of anisotropic hydraulic conductivity at the (small) sub-element scale and at the (large) supra-element scale with anisotropy in statistical moments and correlation lengths.

Another simplification made in the case study is related to strike and dip. Observations from the tunnel indicate that most of the highly permeable structures are not vertical. However, the most serious leakage came from vertically oriented fractures. Thus, with respect to leakage, a vertical fracture zone represents the worst case. An easy way to include the impact of dip is simply to reduce the gravity as cosine to the dip angle, but this is a minor extension that is not included in this study. Furthermore, the fracture zone is simplified to a 2D vertical body with variable hydraulic properties along the fracture zone (x-direction) and with depth (z-direction). Across the fracture zone (y-direction), the hydraulic properties are kept constant. This approach is justified because the spatial extension of the fracture zone is much larger in the x- and z-directions compared to the y-direction. However, by reducing the problem from 3D to 2D, the freedom of flow is drastically reduced: it is always easier to pass a barrier in 3D than in 2D if the barrier has a finite spatial extension. Hence, the effect of preferential flow is underestimated by a reduction from 3D to 2D. This underestimation has serious consequences for measures like artificial infiltration, especially if the infiltration segment of the well does not penetrate the whole fracture zone. The simulations presented in this case study correspond to fully penetrating infiltration wells. Thus a 2D evaluation is most likely too optimistic with respect to the effect of artificial water-infiltration and probably underestimates the amount of water consumption.

In the numerical experiments presented above, the effect of artificial infiltration was analyzed by a simplified simulation setup. A critical point is the set of boundary conditions (b). The simulated water leakage $Q^{(b)}$ may come from two sources: (1) directly from precipitation I_p through the two small lakes and the stretch of boggy land between; or (2) from other indirect sources, such as the distant boggy areas of Kjerringmyra or other interconnected fracture zones. The proportion of water coming from these two sources was kept constant, $I_p=(2/3)Q^{(b)}$. This assumption should be further examined by a sensitivity analysis. Furthermore, the size of the infiltration wells may easily be simulated more realistically by application of a refined local grid. In the present numerical experiments, artificial water infiltration was simulated by applying a constant pressure (P_c=2 bar above the hydrostatic pressure) in a cell with a cross-sectional area of 5×5 m. In reality, P_c is imposed in injection wells with much smaller radii, but the pressure distribution in a rock volume of 5×5 m is hardly uniform. The refinement of this small-scale pressure distribution, however, is beyond the scope of this paper and is also left as a subject for further study.

In this study, hydraulic conductivity for homogeneous fracture zones was calibrated to reproduce hydraulic head and given leakage discharge into the tunnel. A heterogeneous fracture zone with the same expected value as the homogeneous fracture zone was subsequently entered with the standard deviation of permeabilities introduced as a variable. For each case, the effect of artificial water infiltration was evaluated. An alternative approach would be to calibrate $E[K]$ for each permeability field and for each σ_K to get simulated tunnel leakage equal to Q_0, and subsequently to evaluate the impact of artificial water-infiltration. Indirectly, this effect is obtained in the analysis presented herein by relating the influence of artificial infiltration to Q_0 and effective reduction of leakage.

Increasing the variance $var[K]=\sigma_K^2$, while keeping the expectation of K constant $E[K]=\mu_K$, implies that minor parts of the rock volume are assigned increased hydraulic conductivity, whereas major parts become more impervious. This relation is illustrated in Fig. 3, which shows that an increase in frequencies of low hydraulic conductivities is balanced by a minor increase in frequencies of extremely high hydraulic conductivities. If equal quantities of water are conducted through the same rock volume, preferential flow evolves as standard deviation of the hydraulic conductivity increases. The purpose of sealing injection is to plug the most conductive flow paths. However, if an injection well is emplaced in a low-permeable zone, high injection pressure may result in hydraulic fracturing, which increases the permeability. This combined effect of reducing permeability of high-conductive zones and increasing the permeability of low-conductive zones corresponds to a decreased variance of a log-normal pdf while keeping the expected value constant. Hydraulic fracturing of impervious rock volumes is expected to have only local effect around the well. On the other hand, injection of grouting chemicals may have both local and distant effects. In highly conductive channels, grouting may be transported far from the injection well. The perturbation of the log-normal pdf, as made in this study, may indicate the effect of chemical-sealing injection. Regardless of influence volumes, the intention with chemical-sealing injection is to make the permeability in the fracture zone more homogeneous. Homogenization of a heterogeneous fracture zone can be modeled as a decrease of variance. Accepting these arguments, Tables 1 and 2 show that chemical-sealing injection increases the effect of artificial infiltration of water.

 DOI 10.1007/s100400000089

Conclusions

The purpose of the numerical experiments was to demonstrate the impact of increased variance of hydraulic conductivity $K(\mathbf{u})$ on the flow regime. The intention was not to produce statistical moments based on Monte Carlo simulations in this case study, but to illustrate specific flow characteristics for individual realizations with different variance of $K(\mathbf{u})$. Efforts were made to choose a simple simulation setup with boundary conditions corresponding as closely as possible to the observations. From the numerical experiments, a conclusion is that due to significant spatial variability the probability of finding the most important water-conducting channels is very low. For one single realization, the effect of individual infiltration wells in reducing leakage into the tunnel ranges from 28% for the least successful well to 81% for the most successful well (Table 2). However, in locations where artificial infiltration of water potentially has significant effects, the probability of pumping water from the tunnel directly to the surface increases. Relative to effective reduction of leakage, artificial infiltration of water consumes large amounts of water, according to the simulations (Table 1). Since the infiltration equipment in this case is proposed to run on a permanent basis, the cost of water should be taken into account. Based on these numerical experiments, for fracture zones that have a highly variable permeability field, artificial infiltration of water from the tunnel is an uncertain remediation measure. Chemical sealing, however, simulated as a decreased spatial variance of hydraulic conductivity, is favorable for remediation of groundwater pressure. Careful monitoring of the potentially affected area is recommended.

Acknowledgments Thanks to the Norwegian State Railway (NSB) expert panel for open discussions on the problems in the Romeriksporten tunnel, and to Kaare Høeg and Joel Geier for critical and constructive comments. Financial support from the Research Council of Norway and the Norwegian Water Resources and Energy Directorate is gratefully acknowledged.

References

Baveye P, Sposito G (1984) The operational significance of the continuum hypothesis in the theory of water movement through soils and aquifers. Water Resour Res 20:521–530

Bear J (1993) Modeling flow and contaminant transport in fractured rocks. In: Bear J, Tsang C-F, de Marsily G (eds) Flow and contaminant transport in fractured rock. Academic Press, San Diego, pp 1–37

Bear J, Tsang C-F, de Marsily G (1993) Flow and contaminant transport in fractured rock. Academic Press, San Diego

Bour O, Davy P (1998) On the connectivity of three-dimensional fault networks. Water Resour Res 34:2611–2622

Bratvedt F, Bratvedt K, Bucholtz CF, Gimse T, Holden L, Holden H, Risebro NH (1992) Front tracing for groundwater simulations. In: Russel TF, Ewing RE, Brebbia CA, Grey WG, Pinder GF (eds) Computation Methods in Water Resources. Elsevier, pp 97–106

Bratvedt F, Bratvedt K, Bucholtz CF, Gimse T, Holden H, Holden H, Olufsen R, Risebro NH (1994) Three-dimensional reservoir simulation based on front tracing. North Sea Oil and Gas Reservoirs – III. Kluwer Academic Publishers, Dordrecht, pp 247–257

Braud I, Obled C (1991) On the use of empirical orthogonal function (EOF) analysis in the simulation of random fields. Stoch Hydrol Hydraul 5:125–124

Broch E, Kjørholt H (1994) Verification of large-scale permeability tests in hard rocks. Appl Hydrogeol J 2:9–16

Broch E, Elvøy J, Øvstedal E (1997) Romeriksporten – evaluation of a concept study to restore the groundwater balance in the Lutvann-Puttjern area (in Norwegian), Norwegian University of Science and Technology, Trondheim

Christakos G (1992) Random field models in earth sciences. Academic Press, San Diego

Clemo T, Smith L (1997) A hierarchical model for solute transport in fractured media. Water Resour Res 33:1763–1783

Dagan G (1989) Flow and transport in porous formations. Springer, Berlin Heidelberg New York

Damsleth E, Holden L (1994) Mixed reservoir characterization methods. SPE 27969. Proc of University of Tulsa Centennial Petroleum Engineering Symposium, Tulsa, 29–31 Aug

Davenport WB, Root WL (1958) An introduction to the theory of random signals and noise. McGraw-Hill, New York

Gardermobanen (1998) Romeriksporten – application after watercourse legislation § 107.3 on change in licence conditions for Lutvann and Puttjernsonen (in Norwegian), Concession note 33/97, Norwegian Water Resources and Energy Directorate, Oslo

Gelhar LW (1987) Applications of stochastic models to solute transport in fractured rocks. Technical Rep 87–05, Swedish Nuclear Fuel and Waste Management Co, Stockholm

GeoQuest (1998) FRONTSIM/GRIDSIM – user manual. Schlumberger GeoQuest simulation software development. GeoQuest, Lysaker

Gottschalk L (1995) Stochastic hydrology (in Swedish). Lecture notes. Department of Geophysics, University of Oslo, Oslo

Graversen O (1984) Geology and structural evolution of the Precambrian rocks of the Oslofjord-Øyeren area, southeast Norway. Geol Surv Norway Bull 398:1–50

Feder J (1988) Fractals. Plenum Press, New York

Heimli P (1994) NSB (Norwegian State Railways) Gardermobanen–Parcel Oslo S-Nitelva, Tunnel Etterstad-Stalsberg (in Norwegian). Geological report. Noteby, Oslo

Hjort NL, Omre H (1993) Topics in spatial statistics. Rep 871, Norwegian Computing Center, Oslo

Journel AG, Huijbregts ChJ (1989) Mining geostatistics, 4th edn. Academic Press, London

Kitterød N-O, Gottschalk L (1997) Simulation of normal distributed smooth fields by Karhunen-Loève expansion in combination with kriging. Stoch Hydrol Hydraul 11:459–482

Kitterød N-O, Colleuille H, Pedersen TS, Langsholt E, Dimakis P (1998) Water transport in fractured rock, numerical simulation of water leakage in Romeriksporten (in Norwegian). Publ 11, Norwegian Water Resources and Energy Directorate, Oslo

Kjørholt H, Broch E (1992) The water curtain – a successful means of preventing gas leakage from high-pressure, unlined rock caverns. Tunneling Underground Space Tech 7:127–132

Long JCS, Billaux DM (1987) From field data to fracture network modeling: an example incorporating spatial structure. Water Resour Res 23:1201–1216

Mandelbrot BB (1971) A fast fractional Gaussian noise generator. Water Resour Res 7:543–553

Mualem Y (1976) A new model for predicting the hydraulic conductivity of unsaturated porous media. Water Resour Res 12:513–522

National Research Council (1996) Rock fractures and fluid flow. Contemporary understanding and applications. National Academy Press, Washington, DC

 DOI 10.1007/s100400000089

Neretnieks I (1993) Solute transport in fractured rock – applications to radionuclide waste repositories. In: Bear J, Tsang C-F, de Marsily G (eds) Flow and contaminant transport in fractured rock. Academic Press, San Diego, pp 39–127

Norwegian State Railways (1998) Romeriksporten – status of measurements, results and analyses regarding water balance and other enterprises in Østmarka 30/06/98 (in Norwegian). Norwegian State Railways (NSB) – Gardermobanen AS, Oslo

Norwegian Water Resources and Energy Directorate (1987) Runoff maps, Norway, period 1930–1960, 1:500,000 (in Norwegian). Norwegian Water Resources and Energy Directorate, Oslo

Odling NE (1997) Scaling and connectivity of joint systems in sandstones from western Norway. J Struct Geol 19:1257–1271

Oftedahl C (1981) Norway's geology, an overview of Norwegian regional geology, 2nd edn. (in Norwegian). Tapir, Trondheim

Pedersen TS (1997) Tracer test Northern Puttjern/Romeriksporten – preliminary report (in Norwegian). Norwegian Water Resources and Energy Directorate, Oslo

Rohr-Torp E (1994) Present uplift rates and groundwater potential in Norwegian hard rocks. Geol Surv Norway Bull 426:47–52

Sørensen R, Bakkelid S, Torp B (1997) Crustal uplift in Norway. National atlas for Norway (in Norwegian). Norwegian Mapping Authority, Hønefoss

Tsang C-F, Neretnieks I (1998) Flow channeling in heterogeneous fractured rocks. Rev Geophys 36:275–298

 DOI 10.1007/s100400000089